Activation and repolarization of the normal human heart under complete physiological conditions

Charulatha Ramanathan*, Ping Jia*, Raja Ghanem*, Kyungmoo Ryu*, and Yoram Rudy†‡

*Biomedical Engineering, Case Western Reserve University, Cleveland, OH 44106; and †Cardiac Bioelectricity and Arrhythmia Center, Washington University, St. Louis, MO 63130

Communicated by Charles S. Peskin, New York University, New York, NY, February 27, 2006 (received for review October 24, 2005)

Knowledge of normal human cardiac excitation stems from isolated heart or intraoperative mapping studies under nonphysiological conditions. Here, we use a noninvasive imaging modality (electrocardiographic imaging) to study normal activation and repolarization in intact unanesthetized healthy adults under complete physiological conditions. Epicardial potentials, electrograms, and isochrones were noninvasively reconstructed. The normal electrophysiological sequence during activation and repolarization was imaged in seven healthy subjects (four males and three females). Electrocardiographic imaging depicted salient features of normal ventricular activation, including timing and location of the earliest right ventricular (RV) epicardial breakthrough in the anterior paraseptal region, subsequent RV and left ventricular (LV) breakthroughs, apex-to-base activation of posterior LV, and late activation of LV base or RV outflow tract. The repolarization sequence was unaffected by the activation sequence, supporting the hypothesis that in normal hearts, local action potential duration (APD) determines local repolarization time. Mean activation recovery interval (ARI), reflecting local APD, was in the typical human APD range (235 ms). Mean LV apex-to-base ARI dispersion was 42 ms. Average LV ARI exceeded RV ARI by 32 ms. Atrial images showed activation spreading from the sinus node to the rest of the atria, ending at the left atrial appendage. This study provides previously undescribed characterization of human cardiac activation and repolarization under normal physiological conditions. A common sequence of activation was identified, with interindividual differences in specific patterns. The repolarization sequence was determined by local repolarization properties rather than by the activation sequence, and significant dispersion of repolarization was observed between RV and LV and from apex to base.

noninvasive electrocardiographic imaging | normal cardiac activation and repolarization | normal sinus rhythm

Understanding normal cardiac excitation provides a necessary baseline for understanding abnormal cardiac electrical activity and rhythm disorders of the heart, a major cause of death and disability. So far, knowledge of normal human cardiac excitation has been obtained mostly through extrapolation from animal studies, including canine (1, 2) and chimpanzee (3). In addition, human data have been obtained from intraoperative epicardial mapping (4–7) and isolated human hearts (8). Extrapolation of animal studies to humans is limited by interspecies differences in anatomy and electrophysiology. Also, the animal and human studies were conducted under nonphysiological conditions (e.g., anesthesia effects and heart exposure during intraoperative mapping; effects of isolation and absence of neural inputs, mechanical loading, and normal perfusion in isolated heart studies). Until now, it has not been possible to study cardiac excitation in intact healthy subjects under normal physiological conditions because of the unavailability of a noninvasive imaging modality for cardiac electrical function. Electrocardiographic imaging (ECGI) (9) is a noninvasive cardiac electrical imaging modality that can image epicardial potentials, electrograms, and isochrones (activation sequences) using electrocardiographic measurements from many body surface locations together with heart–torso geometry obtained from computed tomography (CT). This imaging technique was extensively validated previously in normal and abnormal canine hearts (10–14). In a recent technical report (9), we introduced the methodology of ECGI application in humans, using single examples of ventricular and atrial activation in a normal subject and in patients with right bundle branch block, ventricular pacing, and atrial flutter. More recently, human ECGI was further validated by comparison to direct epicardial mapping during open-heart surgery in cardiac patients (15) and to catheter mapping in a patient during ventricular tachycardia (16). Following the successful validation of methodology, we report here on a physiological study using ECGI as a noninvasive research tool. We use ECGI to image normal human cardiac activation and repolarization *in vivo* in seven (four males and three females) intact healthy adults under completely normal physiological conditions. We describe common patterns and identify interindividual differences among subjects.

Results

Ventricular Activation. In the normal heart, the cardiac impulse is conducted from the atrioventricular node to the ventricles through the right and left bundle branches of the conduction system. The Purkinje network and the anisotropic fiber structure establish a broad activation front that propagates from endo- to epicardium. Epicardial breakthroughs occur when the activation front arrives at the epicardium and breaks through the surface. The timing and location of these events provide key information on the sequence of ventricular activation.

Epicardial Potentials. The first breakthrough occurs in right ventricular (RV) anterior–paraseptal region during early QRS and is termed RV breakthrough (RVB). Its timing and location are salient features of normal RV activation. In Fig. 1*A Right*, the activation front is represented as a dipole layer (17) approaching RV epicardium, generating a positive potential region (+ sign). ECGI imaged this positive region noninvasively in all subjects; an epicardial potential map from subject no. 1 (Fig. 1*A Left*) is shown as a representative example. Upon breakthrough (Fig. 1*B*), the positive region is invaded by a local potential minimum [blue, −, at the RVB site (Fig. 1*B Left*)]. As shown schematically in Fig. 1*B Right*, this minimum is generated by diverging dipoles that generate negative potentials. The RVB minimum was imaged in all subjects; the times of its appearance are provided in Table 1.

After RVB, additional breakthrough minima appear on RV and left ventricular (LV) epicardium (1). Fig. 1 *C* and *D* show ECGI epicardial potential maps during middle and late QRS

Conflict of interest statement: C.R., P.J., R.G., and Y.R. are coinventors on patents related to ECGI. Their intention is to be involved in a startup company to make ECGI a clinical tool.

Abbreviations: ECGI, electrocardiographic imaging; CT, computed tomography; RV, right ventricle/ventricular; RVB, RV breakthrough; LV, left ventricle/ventricular; ARI, activation recovery interval; APD, action potential duration.

‡To whom correspondence should be addressed. E-mail: rudy@wustl.edu.

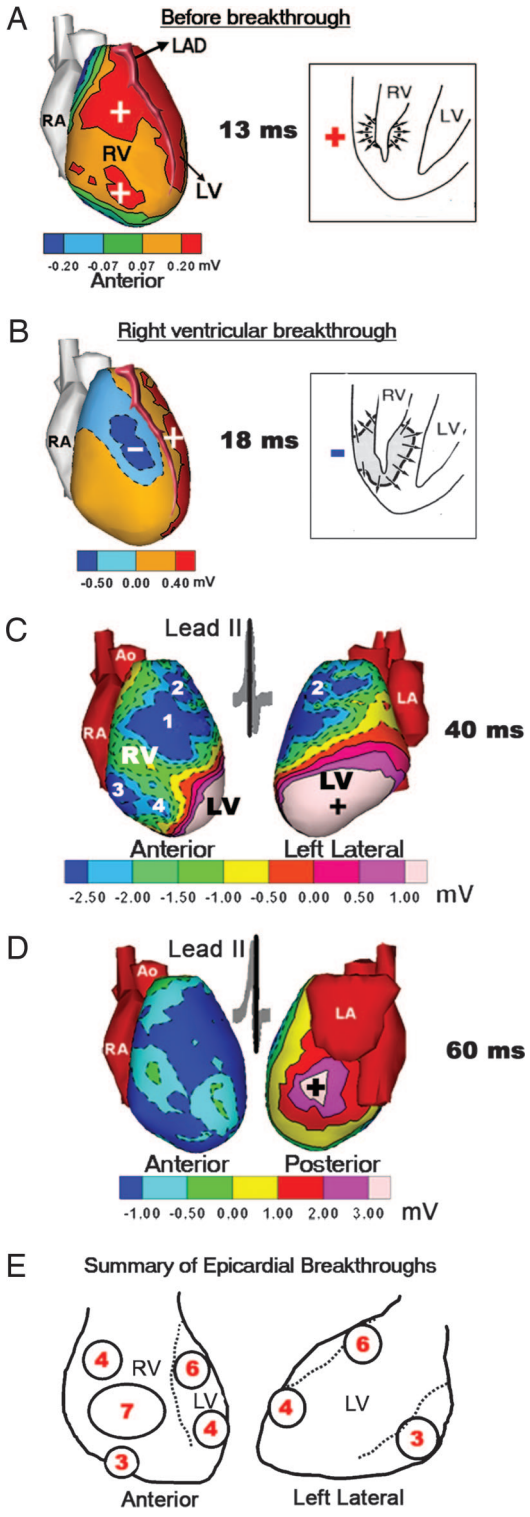

Fig. 1. Epicardial potentials during ventricular activation (subject no. 1). (*A*) Five milliseconds before epicardial breakthrough. Cartoon (*Right*) represents activation front as a dipole layer approaching the RV epicardium generating positive potentials (+ sign). Positive potentials and local maxima cover the RV (*Left*). (*B*) RVB. Upon breakthrough, a local intense potential minimum (blue, −) appears at the breakthrough site (*Left*); the cartoon (*Right*) shows a schematic of the activation front and dipole source distribution at this time. (*C*) Epicardial potential map during the middle of QRS (40 ms; Lead II of ECG is shown for timing). Multiple breakthroughs are seen (minima, dark blue): RVB, labeled 1; left-anterior-paraseptal breakthrough, labeled 2; inferior-RVB, labeled 3; and apical breakthrough, labeled 4. Lateral view shows extensive maximum on LV apex (+ sign). (*D*) Epicardial potential map during late QRS (60 ms; see Lead II). Apical maximum seen at 40 ms has migrated towards LV posterolateral base (posterior view). (*E*) Summary of early activation sites imaged by ECGI. Numbers and their corresponding locations indicate number of subjects that had a breakthrough at that location. RV, right ventricle; LV, left ventricle; Ao, aorta.

using subject no. 1 as a representative example. During mid-QRS (Fig. 1*C Left*), more breakthroughs appear in the left-anterior-paraseptal region (Fig. 1*C Left*, *2*), right-inferior RV (Fig. 1*C Left*, *3*), and apical RV region (Fig. 1*C Left*, *4*). Note well developed RVB minimum (Fig. 1*C Left*, *1*) that has spread in all directions. Minimum at site 2 [also observed by Durrer *et al*. (8) in isolated hearts] is attributed to an activation front generated by the left-anterior fascicular branch of the left bundle branch (7). Subsequent time frames (not shown) show further development and spread of the breakthrough minima. At QRS end (Fig. 1*D Left*), RV is engulfed in negative potentials because of the coalescence of all breakthrough minima. Thus normal epicardial RV activation is caused by the coalescence of multiple breakthroughs, an observation consistent with high-resolution mapping of canine epicardium (1).

On the LV, a broad maximum develops over the lateral-apical region (Fig. 1*C Right*), reflecting endocardial-to-epicardial propagation of the LV free-wall activation front (8). We observed from epicardial potential maps of subsequent times (epicardial potential movie in Movie 1, which is published as supporting information on the PNAS web site) that this maximum migrated from lateral LV apex toward the posterolateral base. This is also evident from LV potential distribution at QRS end (Fig. 1*D Right*), where the apical maximum of Fig. 1*C* has become localized and moved to posterobasal LV (last to activate). Interindividual differences in the last areas to activate are presented in Table 1.

Fig. 1*E* presents a summary of all imaged epicardial breakthroughs in all seven subjects. Overall, there is good agreement between these breakthrough sites and those observed in an intraoperative study of early activation sites by Wyndham *et al.* (7).

Ventricular Electrograms. Fig. 2 shows typical normal electrograms imaged by ECGI using subject no. 1 as a representative example. Electrograms are shown from select RV and LV locations (Fig. 2*A*, *1–8*). Circles on the electrograms indicate activation times. Anterior RV electrograms (RVB region, Fig. 2*B*, *1*) show rS morphology; the r wave component (<0.7 mV) reflects early left-to-right septal activation (8, 18) and RV free-wall activation, the sharp rS downslope reflects local epicardial RV activation, and the rest of the S wave reflects continued RV activation and remote LV activation (5, 6). Toward RV apex (Fig. 2*B*, *2*), Rs morphology is reconstructed, with local activation on the Rs downslope. Superior RV (RV outflow tract, Fig. 2*B*, *3*) typically shows rSr′ morphology, with local activation time on later r′-wave. Posterior RV (Fig. 2*B*, *4*) also shows rS morphology. Thus, anterior-paraseptal, apical, posterior, and superior RV epicardium always exhibit waveforms that are amplitude variations of RS or rSr′ morphology, in agreement with intraoperative mapping in humans (5, 6).

In LV, the region adjacent to the anterior interventricular septum typically shows electrograms of rS morphology (Fig. 2*B*, *5*). Increasing amplitude R waves (Fig. 2*B*, *6*) are observed closer to the LV apex. Except anterior and anterolateral regions, most LV electrograms exhibit initial q wave (<30-ms duration) reflecting rightward septal activation (Fig. 2*B*, *7* and *8*). In some subjects, this q wave is reflected more apically. Thus, LV electrograms from free-wall (Fig. 2*B*, *7*) and posterior (Fig. 2*B*, *8*) are variants of qR or qRs morphology, consistent with direct mapping (5, 6).

Table 1. Pooled data comparisons

Subject no.	Age/gender	QRS duration, ms	RVB time, ms	Last area to activate	Mean ARI, ms	ARI dispersion, ms
1	27/F	90	18	LV base	256	30
2	26/F	91	19	RVOT	220	40
3	22/M	85	21	RVOT/LV base	230	47
4	43/M	98	22	LV base	248	52
5	28/F	76	24	LV base	231	43
6	22/M	100	21	RVOT	200	39
7	28/M	95	20	LV base	260	48

Age, gender, and QRS duration (determined from the 12-lead electrocardiogram used for subject selection). Times of earliest activation (RVB), last area to activate, mean activation recovery intervals (ARI), and ARI dispersion (LV apex-to-base) were determined from ECGI images. F, female; M, male. RVOT, RV outflow tract.

Ventricular Isochrones. In Fig. 3, we present ventricular isochrone maps of three subjects (Fig. 3 *A–C*). Two adjacent early activation sites on a line perpendicular to the left anterior descending coronary artery (LAD) are imaged in subject no. 1 (Fig. 3*A*, *1, 2*). Posterior LV activation of this subject shows uniform isochrones, with posterolateral LV being last to activate. In subject no. 3 (Fig. 3*B*), an elongated early activation region (Fig. 3*B*, *1*) parallel to the LAD is observed. We also imaged early activation in the left-anterior-paraseptal region (Fig. 3*B*, *2*). In subject no. 4 (Fig. 3*C*), several early epicardial activation (breakthrough) sites are seen: *1*, RVB; *2*, left paraseptal; *3*, left apical; and *4*, posterior LV. Uniform isochrones on posterior LV, ending at the LV base, are observed in subjects nos. 1 and 3. In all subjects, the LV base is the last to activate, and epicardial slow propagation

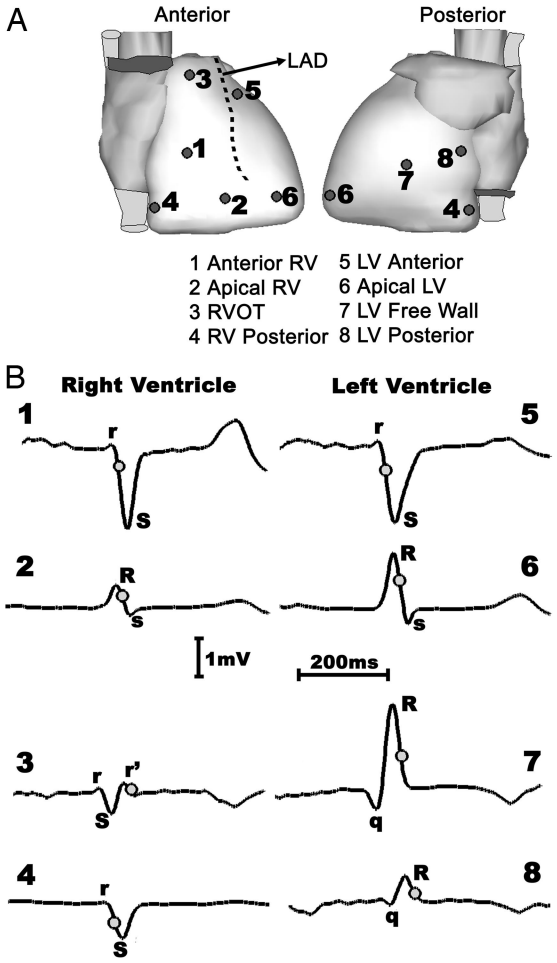

Fig. 2. Morphology of selected electrograms over entire RV and LV. (*A*) Anterior and posterior heart outlines showing electrogram locations (anatomical positions listed below). (*B*) Electrograms from subject no. 1 from RV locations 1–4 (*Left*) and from LV locations 5–8 (*Right*). RVOT, RV outflow tract.

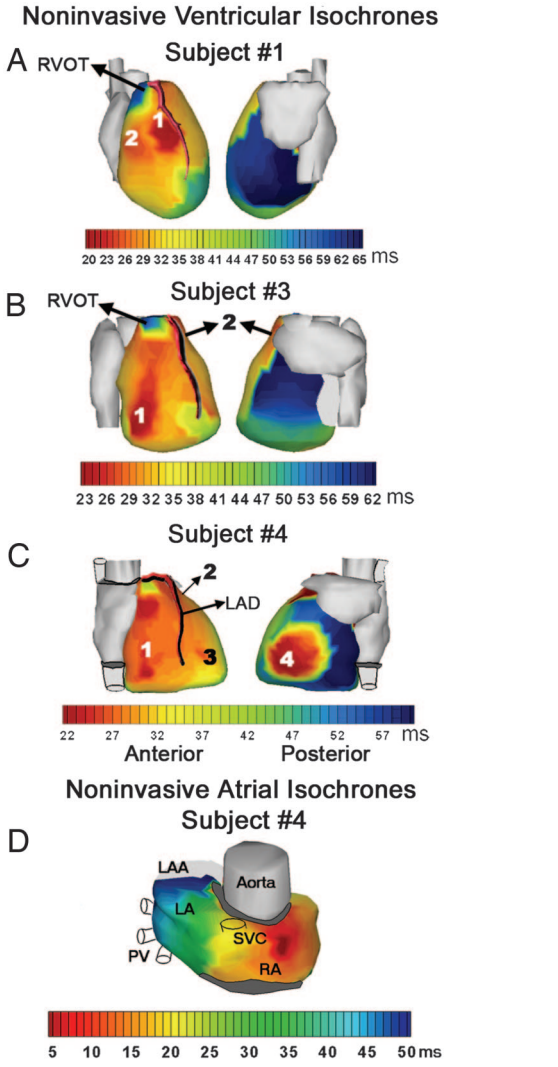

Fig. 3. Ventricular and atrial isochrones. Ventricular epicardial isochrones from subjects nos. 1 (*A*), 3 (*B*), and 4 (*C*). Numbers indicate location of early activation sites (adapted from figure 2*C* of ref. 9). (*D*) Atrial activation isochrones from subject no. 4. LAA, left atrial appendage; PV, pulmonary veins; SVC, superior vena cava. RVOT, RV outflow tract.

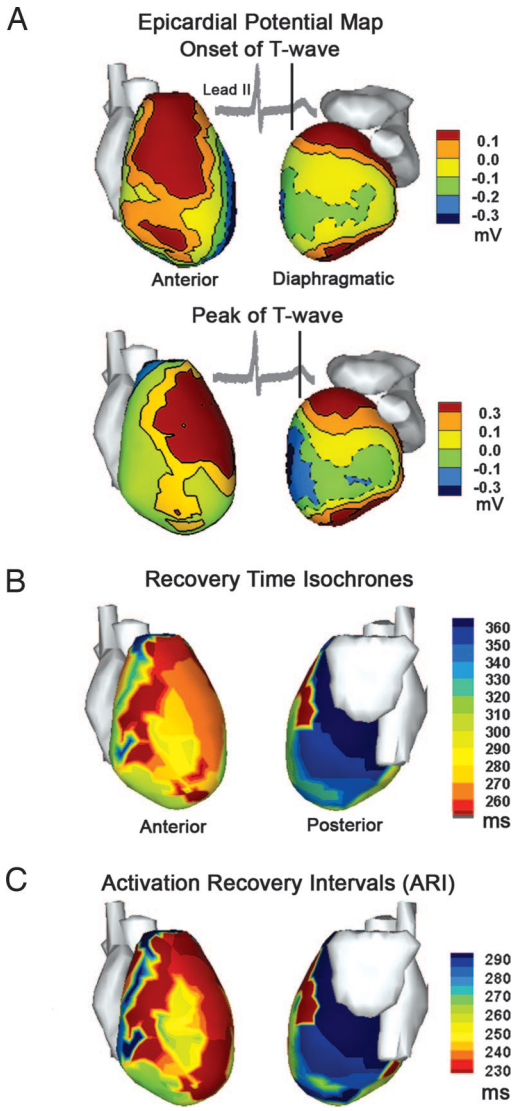

Fig. 4. Ventricular repolarization (subject no. 1). (*A*) Anterior and diaphragmatic views of epicardial potential maps during T wave. Maps during T wave onset (*Upper*) and peak (*Lower*) are shown (see Lead II for timing). (*B*) Epicardial recovery-time isochrones. (*C*) Epicardial ARI map.

(crowded isochrones) is seen in the RV outflow tract region. Pooled data comparisons of ventricular activation characteristics (QRS durations, RVB times, and last areas to activate) among subjects are provided in Table 1.

Atrial Isochrones. Fig. 3*D* shows ECGI images of atrial activation isochrones from subject no. 4. Earliest activation (deep red) starts in right atrium (RA), near the attachment of the superior vena cava (the anatomical location of the sinoatrial node), where the impulse originates. The impulse propagates to the rest of the RA and left atrium (LA). LA appendage is activated last. These imaged isochrones are consistent with those recorded directly in isolated human hearts (8).

Ventricular Repolarization. In contrast to the dynamic pattern of epicardial potentials during depolarization (QRS), epicardial potential patterns of normal repolarization hardly vary during the ST-T segment. This static pattern reflects the relatively slow process of repolarization, which, unlike the localized and propagated depolarization process, covers the entire ventricular myocardium. We describe T wave epicardial potential patterns using subject no. 1 as a representative example (Fig. 4). During T wave onset, a maximum (dark red) appears over the anterior surface (Fig. 4*A Upper*); it remains static and intensifies during peak T wave (Fig. 4*A Lower Left*). Negative potentials (green and blue) cover most of the apical and inferior LV and persist through T wave peak (Fig. 4*A Right*). These human patterns are consistent with T wave patterns in the chimpanzee heart (3).

The electrograms in Fig. 2 clearly indicate that ECGI can reconstruct epicardial T waves. Typically, anterior RV electrograms show upright T waves, whereas posterior and apical LV show negative T waves. These reconstructed human T wave morphologies are very similar to those observed in the chimpanzee (3). A recovery-time isochrone map is shown in Fig. 4*B* (all times are from QRS onset). The corresponding activation recovery interval (ARI) (14) map is shown in Fig. 4*C*. In general, recovery times are determined by both the activation sequence and local repolarization, whereas ARIs reflect only the local repolarization and local action potential duration (APD), independent of the activation sequence. The close correlation between the recovery-time isochrone map (Fig. 4*B*) and the ARI map (Fig. 4*C*) indicates that local APD (local repolarization) is the major determinant of the repolarization sequence in the normal human heart. The much lower similarity to the activation-time isochrone map of the same subject (Fig. 3*A*) indicates a minor role for the activation sequence in determining the repolarization sequence, an observation also documented by direct mapping in normal canine hearts (19). This property of normal repolarization results from the fast spread of activation in the normal heart, where the Purkinje system plays a major role. Normally, spatial differences in activation times are much smaller than in APD, and local APD determines the local repolarization time to a very close approximation. For subject no. 1, mean ARI over ventricular epicardium is 256 ms (maximum, 329 ms; minimum, 191 ms). The difference between LV and RV average ARI (LV-RV averaged over all reconstructed RV and LV ARIs in subject no. 1) is 32 ms. Apex-to-base LV ARI dispersion is 30 ms and shows uniform gradation (Fig. 4*C Right*, green to blue). Table 1 summarizes ARI mean values and apex-to-base dispersions for all subjects. Note that mean ARI values are in the range of typical human APDs. Dispersions are between 30 and 52 ms. Mean ARI and dispersion averaged over all subjects were 235 and 42 ms, respectively.

Discussion

This study characterizes normal atrial activation and ventricular activation and repolarization in the intact human heart under normal physiological conditions, using a noninvasive imaging modality called ECGI. Because ECGI is noninvasive, it has enabled us to study normal activity under complete physiological conditions (closed chest, no anesthesia, presence of neural inputs, mechanical loading, and normal perfusion) in intact human subjects. The study was conducted in seven healthy adults using ECGI to image epicardial potentials, electrograms, and isochrones. Similar to invasive epicardial mapping, ECGI images are limited to the heart's surface. Before epicardial breakthrough, epicardial potentials and electrograms reflect intramural excitation. Based on a knowledge of anatomy, its role in the excitatory process, and published intramural recordings (8, 18, 20), intramural activity can be inferred from ECGI epicardial information (11, 13). This property has been demonstrated in canine hearts (11, 13). For example, during pacing, ECGI was able to estimate intramural depth of pacing sites (simulating intramural ectopic foci) (11), and in an infarcted canine heart, ECGI provided information on intramural components of reentry during ventricular tachycardia (13). Other approaches have been developed to image intramural activation. Modre *et al.* (21) imaged myocardial activation using activation time imaging.

More recently, myocardial activation sequences of rabbit hearts during ventricular pacing were imaged by Zhang *et al.* (22).

Normal activation is conducted to the ventricles through both bundle branches of the conduction system. Anatomically, the right bundle branch is a minimally branched structure, whereas the left bundle branch is more diffuse, with two principal branches, large posterior radiation (posterior fascicle) and smaller anterior radiation (anterior fascicle). There is interindividual variability in this structure and in the distribution and penetration of Purkinje fibers, resulting in significant differences of ventricular activation patterns among individuals. Indeed, in this study, a general sequence of activation common to all subjects is identified, with interindividual differences in specific details of the patterns.

Earliest epicardial activation occurred in RV right-paraseptal region in all subjects; this RVB occurred within 25 ms of QRS onset. Multiple breakthroughs aligned parallel to the left anterior descending coronary artery (LAD) were found in this region (Fig. 3*C*, *1*), as observed in the dog (1). Sometimes a large elliptical area of earliest epicardial activation parallel to LAD was found (Fig. 3*B*, *1*). Before this event, negative potentials or electrogram q waves of duration <30 ms were observed on posterior LV, reflecting left-to-right septal activation and RV free-wall activation (Fig. 2*B*, electrograms from sites *7* and *8*). An average 7 ms after occurrence of RVB, LV breakthroughs occurred on the anterior-paraseptal region (all subjects) or posterior LV (subject no. 4, site 4). Simultaneously with or subsequent to this event, multiple breakthroughs on the RV appeared, typically near RVB and on inferior RV (three subjects). Subsequently, another LV breakthrough appeared on apical anterior LV (four subjects). In all subjects, all breakthroughs appeared <40 ms from ventricular activation onset. Most RV epicardium was depolarized by the coalescence of various breakthroughs on the RV. LV activation was achieved through a combination of: (*i*) transmural conduction, (*ii*) radial spread from breakthrough sites, (*iii*) spread from RV, and (*iv*) spread from apex. Typically, a region of colliding wavefronts (R wave electrograms in Fig. 2*B*, *6*) was observed on the left-anterior margin. The latest activation occurred in posterior or posterolateral basal LV and/or RV outflow tract. ECGI images of atrial activation during normal sinus rhythm were consistent with direct human atrial mapping (8). Isochrone maps showed radial spread from the sinus node with the latest activation of the left atrial appendage.

In many ways, this *in vivo* study in seven normal, intact, and awake adults is the physiological counterpart, under complete physiological conditions, of the classic study by Durrer *et al.* (8) in seven isolated human hearts. In Durrer's study, the hearts were isolated from seven individuals who died from various cerebral noncardiac causes. Obviously, activation in these hearts was not studied under completely normal physiological conditions; nonphysiological effects included lack of neural inputs and mechanical loading, nonphysiologic perfusion, exposure to a medium (volume conductor) with different properties than *in vivo*, and possible damage caused by the isolation procedure and insertion of needle electrodes. Such difficulties are unavoidable in isolated heart experiments. The present study takes advantage of the noninvasive nature of ECGI to obtain data that are free from the nonphysiological effects associated with the isolation procedure.

Conduction velocities of ventricular epicardial activation estimated from epicardial isochrone maps were often nonphysiologically high (>1,000 cm per sec). This is because velocity measured on the epicardial surface is a true velocity only when the wavefront is perpendicular to the surface (1). In dog hearts (1), it was observed that, where the wavefront was at an angle to the surface, measured epicardial velocities had a wide range (100–1,100 cm per sec). Clearly, these apparent (pseudo) velocities can reach very high values; at the extreme, a wavefront parallel to and traveling toward the surface can generate simultaneous activation of a large epicardial region with an infinite apparent velocity. Similarly, large apparent velocities can result from irregularities in a wavefront approaching the epicardium (23). Estimated atrial conduction velocities were in the physiological range possible for true propagation (80–100 cm per sec), because the thin atrial wall minimizes endocardial to epicardial spread and the associated estimation error.

The ability to image and determine cardiac repolarization is important, because repolarization abnormalities and large dispersions are underlying causes of many arrhythmias (14, 19). Normal ventricular repolarization was characterized by T wave electrograms, potential maps, recovery-time isochrones, and ARI maps. In all cases, the repolarization sequence was determined by local repolarization (APD) with minimal effect of the activation sequence (Fig. 4 *B* and *C*). This is because normal ventricular activation is fast, and spatial differences in activation times are much smaller than APD differences. Thus, to a good approximation, epicardial activation can be assumed to be simultaneous when recovery is considered. This is in contrast to repolarization during ectopic activity or pacing, when the conduction system does not participate. For such activity, conduction is slow, and activation time differences are much longer than APD differences. Under such circumstances, local repolarization time is determined by the activation sequence (9). A gradient of ARIs from RV to LV and from LV apex to base was imaged. Similar gradients were measured in canine hearts (14, 19). The normal canine heart (14) was found to have an average ARI of 200 ms (vs. 235 ms for human hearts in this study). Measured canine LV apex-to-base ARI dispersion was ≈28 ms, and average LV to RV ARI difference was 19 ms. Although repolarization dispersion indices for human epicardium have not been directly mapped, Vasallo *et al.* (24) mapped LV endocardial dispersion of 52 ms.

All presented results are based on intrinsic resting heart rates. A study of the changes in normal activation and repolarization because of increased heart rate (e.g., during exercise) is also of great interest but outside the scope of this paper. Future studies in our laboratory may explore such rate-dependent phenomena using ECGI.

Methods

Mathematical Approach. ECGI reconstructs epicardial potentials, electrograms, and isochrones from body surface potentials using mathematical reconstruction algorithms. The basis for ECGI methodology is the discretization of Laplace's equation, which computes the electrical potential field in the source-free volume between the heart and body surfaces. Application of Green's second theorem and the boundary element method results in a transfer matrix relating body surface potentials to epicardial potentials. Epicardial potentials are then computed from the body-surface potentials applying a constraint-based Tikhonov regularization (25) and/or an iterative GMRes method (26). Details of the mathematical methods have been provided in previous publications (25, 27–29).

Procedure for Human Studies. The subjects selected for the study were healthy adults, in the age range of 21–43 years. Seven subjects (four males and three females; see Table 1) participated in the study. Each subject had a typical normal 12-lead electrocardiogram and no known history of heart disease. Before the study, we obtained informed consent based on the guidelines and regulations of the Institutional Review Board (IRB) of the University Hospitals of Cleveland (UH) and Case Western Reserve University (all our studies were performed at UH). The human research protocol was approved by the

hospital IRB. Details of the procedure were provided in a previous publication (9).

In ECGI, we record 224 electrocardiograms over the entire torso surface and also obtain subject-specific heart–torso geometry using CT. First, a 224-electrode vest was strapped on the subject's torso and connected to a custom-built multichannel mapping system. Torso-surface electric potentials are recorded followed by a thoracic CT scan to obtain high-resolution images of the heart and the vest electrodes. The electrode positions and 3D epicardial surface geometry are obtained via segmentation from each of the transverse CT images. The electric potential and geometry information are then processed by ECGI to obtain, noninvasively, potentials, electrograms, and isochrones over the entire epicardial surface of the heart during the entire cardiac cycle. A block diagram of the ECGI procedure is included in Fig. 5, which is published as supporting information on the PNAS web site.

ECGI reconstructions of epicardial potential maps, electrograms, and isochrones were performed for each subject and analyzed to interpret the sequence of ventricular activation. Epicardial potential maps were reconstructed at 1-ms intervals. Epicardial electrograms, each depicting the variation of potential with time at a single site, were computed at many sites (typically 400–800) over the epicardial surface. Isochrone maps depict the sequence of epicardial activation based on local activation times, taken as the point of maximum negative derivative ($-dV/dt_{max}$) of the QRS segment in each electrogram. We compared the sequence and patterns of reconstructed epicardial potentials, electrograms, and isochrones in each subject with published invasive epicardial recordings from chimpanzee (3) and human hearts [intraoperative (7) and isolated (8)]. Ventricular repolarization was analyzed by using reconstructed epicardial potential maps during the T wave, T wave electrograms, and ARI (14, 30, 31). ARIs were determined as the difference between activation time and recovery time (taken as the dV/dt_{max} of the T wave on the reconstructed electrogram). ARIs are important in the study of repolarization properties as they reflect local APD (30, 31).

We present the results through example maps of individual subjects that are typical and representative of the rest of the subject pool. Pooled data comparisons are presented in Table 1.

We thank Les Ciancibello for his outstanding technical assistance in CT and Elena T. DuPont for her assistance in transporting images from the hospital to our laboratory. This study was supported by National Institutes of Health/National Heart, Lung, and Blood Institute MERIT Award R37-HL-33343 and Grant R01-HL-49054 (to Y.R.). Y.R. is the Fred Saigh Distinguished Professor at Washington University.

1. Arisi, G., Macchi, E., Baruffi, S., Spaggiari, S. & Taccardi, B. (1983) *Circ. Res.* **52,** 706–715.
2. Scher, A. M. (1964) *Am. J. Cardiol.* **14,** 287–293.
3. Spach, M. S., Barr, R. C., Lanning, C. F. & Tucek, P. C. (1977) *Circulation* **55,** 268–278.
4. Barker, P. S., Macleod, A. G. & Alexander, J. (1930) *Am. Heart J.* **3,** 720–742.
5. Jouve, A., Corriol, J., Torresani, J., Benyamine, R., Velasque, P. & Peytavy, R. (1959) *Am. Heart J.* **59,** 856–868.
6. Roos, J. P., van Dam, R. T. & Durrer, D. (1968) *Br. Heart J.* **30,** 630–637.
7. Wyndham, C. R., Meeran, M. K., Smith, T., Saxena, A., Engelman, R. M., Levitsky, S. & Rosen, K. M. (1979) *Circulation* **59,** 161–168.
8. Durrer, D., van Dam, R. T., Freud, G. E., Janse, M. J., Meijler, F. L. & Arzbaecher, R. C. (1970) *Circulation* **41,** 899–912.
9. Ramanathan, C., Ghanem, R. N., Jia, P., Kyungmoo, R. & Rudy, Y. (2004) *Nat. Med.* **10,** 422–428.
10. Oster, H. S., Taccardi, B., Lux, R. L., Ershler, P. R. & Rudy, Y. (1997) *Circulation* **96,** 1012–1024.
11. Oster, H. S., Taccardi, B., Lux, R. L., Ershler, P. R. & Rudy, Y. (1998) *Circulation* **97,** 1496–1507.
12. Burnes, J. E., Taccardi, B. & Rudy, Y. (2000) *Circulation* **102,** 2152–2158.
13. Burnes, J. E., Taccardi, B., Ershler, P. R. & Rudy, Y. (2001) *J. Am. Coll. Cardiol.* **38,** 2071–2078.
14. Ghanem, R. N., Burnes, J. E., Waldo, A. L. & Rudy, Y. (2001) *Circulation* **104,** 1306–1312.
15. Ghanem, R. N., Jia, P., Ramanathan, C., Ryu, K., Markowitz, A. & Rudy, Y. (2005) *Heart Rhythm* **2,** 339–354.
16. Intini, A., Goldstein, R. N., Jia, P., Ramanathan, C., Ryu, K., Giannattasio, B., Gilkeson, R., Stambler, B., Brugada, P., Stevenson, W. G., *et al.* (2005) *Heart Rhythm* **2,** 1250–1252.
17. Rudy, Y. (2000) in *Heart Physiology and Pathophysiology*, eds. Sperelakis, N., Kurachi, Y., Terzic, A. & Cohen, M. (Academic, San Diego), pp. 133–148.
18. Scher, A. M., Young, A. C., Malmgren, A. L. & Erickson, R. V. (1955) *Circ. Res.* **3,** 56–54.
19. Burgess, M. J. (1979) *Am. J. Physiol.* **236,** H391–H402.
20. Taccardi, B., Macchi, E., Lux, R. L., Ershler, P. R., Spaggiari, S., Baruffi, S. & Vyhmeister, Y. (1994) *Circulation* **90,** 3076–3090.
21. Modre, R., Tilg, B., Fischer, G. & Wash, P. (2002) *IEEE Trans. Biomed. Eng.* **49,** 1153–1161.
22. Zhang, X., Ramachandra, I., Liu, Z., Muneer, B., Pogwizd, S. M. & He, B. (2005) *Am. J. Physiol.* **289,** H2724–H2732.
23. Durrer, D. & van der Tweel, L. H. (1953) *Am. Heart J.* **46,** 683–691.
24. Vassallo, J. A., Cassidy, D. M., Kindwall, K. E., Marchlinski, F. E. & Josephson, M. E. (1988) *Circulation* **78,** 1365–1372.
25. Tikhonov, A. N. & Arsenin, V. Y. (1977) *Solutions of Ill-Posed Problems* (Wiley, New York).
26. Calvetti, D., Lewis, B. & Reichel, L. (2002) *Bit* **42,** 44–65.
27. Rudy, Y. & Oster, H. S. (1992) *Crit. Rev. Biomed. Eng.* **20,** 25–45.
28. Rudy, Y. & Burnes, J. E. (1999) *Ann. Noninvasive Electrocardiol.* **4,** 340–358.
29. Ramanathan, C., Jia, P., Ghanem, R. N., Calvetti, D. & Rudy, Y. (2003) *Ann. Biomed. Eng.* **31,** 981–994.
30. Haws, C. W. & Lux, R. L. (1990) *Circulation* **81,** 281–288.
31. Millar, C. K., Kralios, F. A. & Lux, R. L. (1985) *Circulation* **72,** 1372–1379.